International Journal of Health Sciences and Research
Volume 14; Issue: 7; July 2024
Website: www.ijhsr.org
Research Article *ISSN: 2249-9571*

Repercussions on Quinolone Resemblance in Enterotoxigenic *E. coli* gyrA Mutants: Molecular Dynamics Simulations and Residue Interaction Network Analysis

Nitin Jumnani

Alwar Pharmacy College, Alwar

DOI: https://doi.org/10.52403/ijhsr.20240714

ABSTRACT

Regarding foreign travel, particularly to impoverished nations, travelers' diarrhea (TD) is one of the most significant global health challenges. The most common infection causing TD is enterotoxigenic *Escherichia coli* (ETEC). TD is extremely incapacitating, yet it also has a self-limiting effect. For TD patients, ciprofloxacin is one of the common quinolone medications. Finding new medications is urgently needed, though, due to the alarmingly high levels of antibiotic resistance. GyrA, which is only found in prokaryotes and is crucial for bacterial viability, is the pharmacological target of ciprofloxacin. Reduction in affinity for quinolones is explained by increasing quinolone resistance *in vivo*, which is linked to several mutations in the gyrA region that determines quinolone resistance. To gain insight into the molecular processes that underlie the drug resistance mechanism, we provide here, for the first time as far as we are aware, the structural and dynamic impacts of ETEC gyrA mutations on ciprofloxacin affinity relative to the wild-type protein. According to our simulations, mutations drastically change the global dominant motion pattern and the gyrA residue interaction network in the key domains peculiar to the N-terminal regions of gyrA. To treat drug-resistant bacterial illnesses, like TDs, this work offers crucial information for developing more effective anti-bacterial medicines with high ligand efficacy.

Keywords: *Escherichia coli*, ciprofloxacin, gyrA gene, MD simulations, mutation

INTRODUCTION

Higher eukaryotic creatures lack the type II topoisomerase gyrA, which is crucial to bacterial life and a potential target for antibacterial therapy. Due to gyrA's distinct action mechanism of altering DNA topology and its essential character, certain gram-positive and gram-negative bacteria have been exploiting it as a therapeutic target for a long time. One of the two essential subunits of DNA gyrase, it controls DNA supercoiling and aids in DNA unwinding at replication forks [1,2]. The two subunits comprising the heterotetramer (A2B2) DNA gyrase encode the gyrA and gyrB genes, respectively. GyrA and GyrB have respective molecular weights of 97 and 90 kDa. Though a high-resolution structure for the gyrase holoenzyme (A2B2) is not yet available, the X-ray crystal structure of the *E. coli* GyrA59 fragment (PDB ID: 1ab4), which comprises residues 30-522, was solved at a resolution of 2.8 Å [3,4]. Antibacterial medicines with tremendous therapeutic potential target gyrA because of

their ATP-dependent mechanism for forming negative supercoils in DNA. Thus, the most efficacious inhibitors of bacterial topoisomerases have been members of the broad-spectrum antibacterial medication family called quinolones [5,6]. Quinolones are a class of antibiotics that stabilize the covalent enzyme-DNA complex and create DNA lesions that impede vital biological functions including transcription, recombination, and DNA replication. This prevents microorganisms' development [7].

TD is the most prevalent and expensive health problem that strikes visitors to tropical and developing countries. ETEC is the primary cause of most instances [8]. Antibiotics called fluoroquinolones are useful in treating severe instances of TB. Ciprofloxacin is the fluoroquinolone that is prescribed the most frequently out of all of them. Due to the extensive use of quinolone antibiotics, the incidence of *E. coli* bacteria resistant to these drugs has been continuously increasing [9]. The discovery supports the hypothesis that interactions between antibiotics and their targets might contribute to drug resistance. Quinolone resistance rises in tandem with a decrease in the use of antibiotics, plasmid-mediated resistance, and gyrase gene alterations, which are thought to be the most significant in clinical circumstances. These alterations have been restricted to the *E. coli* gyrase subunit A's QRDR domain (residues 67-106) [5,10,11]. Examining the structural consequences of these antibiotic resistance-related mutations may significantly improve our comprehension of the associated molecular changes in the functionally significant regions of the target. Minimum Inhibitory Concentration (MIC) values have been demonstrated to increase in response to S83L and a double mutation S83L/D87N, as well as T86I and a double mutation T86I/P104S, which have been associated with quinolone resistance in ETEC isolates from diarrhea patients across various areas [12,13]. By utilizing molecular dynamic simulation techniques to examine these mutations, it could be feasible to comprehend the molecular process behind the associated abnormalities. The target's structure may change due to these alterations, potentially changing how it functions. A protein's conformational flexibility appears to affect how it interacts with its ligand. This study aimed to examine the dynamic behavior of gyrA in ETEC to provide insight into the molecular changes brought about by the ciprofloxacin resistance-causing mutations S83L and S83L/D87N in ETEC gyrA (Figure 1).

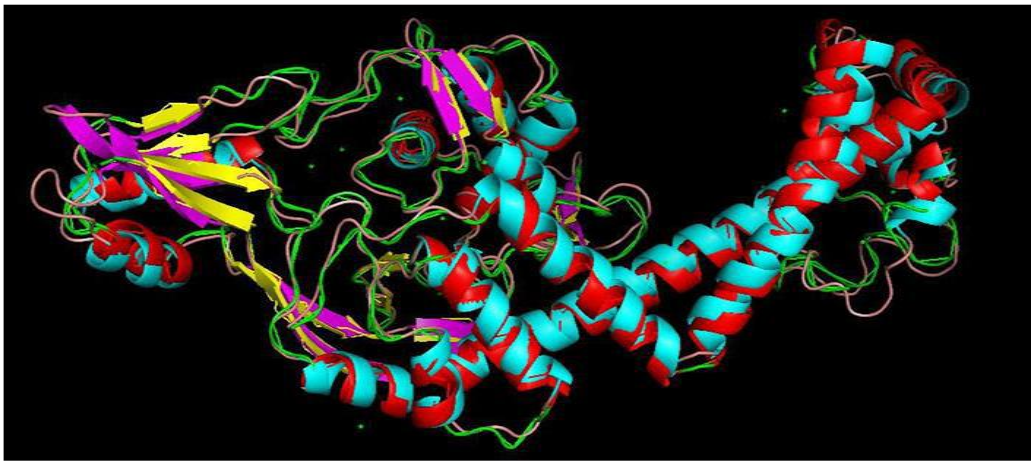

Fig. 1 An illustration of ETEC gyrA that emphasizes its distinct domains, catalytic site, and mutations connected to quinolone resistance in diarrhea patients. In this stick figure, the catalytic region is displayed in cyan, while QRDR mutations are displayed in yellow. The CAP domain is represented by violent purple, the tower by blue, the dimerization domain by orange, and the connecting a-helices by orange.

MATERIAL AND METHODS

Preparation of Ligand

The Ciprofloxacin drug has the PubChem compound identification number 2764. The two-dimensional structure was retrieved from the PubChem Compound database in the SDF format [14]. The structure was tailored to reflect the ionization states of its functional groups within the pH range of 6.5-8.5, considering the predominant dissociation of the carboxylic acid group at pH values over 6.09 and protonation of the nitrogen at pH values under 8.74. The objective of the subsequent conformational search was to pinpoint a set of conformers characterized by minimal energy. A maximum of 10 tautomers and stereoisomers were generated for the ligand. The resulting structure underwent an energy minimization process using the CHARMm force field and the Smart Minimizer Algorithm to ensure structural stability and inform potential interactions with biological targets. Using homology modeling, the gyrA amino acid sequences of *Escherichia coli* O78:H11 (875 aa) were acquired from the Uniprot database under the accession number A7ZP49. The structures were modeled in Discovery Studio and showed 91.2% identification with enterotoxigenic *E. coli* (ETEC), using *E. coli* gyrA (PDB Id: 1AB4) as a template. We utilized DS to build our first homology models. We selected the DS model for each structure with the highest Discrete Optimized Protein Energy (DOPE) score out of five that were produced. The DOPE score can be used to quantitatively assess the overall quality of homology-modeled structures. Following that, we analyzed the models' residue profiles with Verify3D [15] and, PROCHECK [16] to ensure there were no stereo-chemical abnormalities.

We used DS to reduce energy and build both the original and mutant ETEC structures. The mutant-type structures (MT) of ETEC were formed by substituting amino acids at positions 83 and 87 in the wild-type (WT) ETEC gyrA. This resulted in mutants with either a single (S83L) or a double mutation (S83L/D87N). To prepare the receptor architectures, we employed the looper approach to optimize the short and medium loop parts while minimizing the remaining loop areas. We then assigned the appropriate ionization states at physiological pH 7.4 and optimized the hydrogen network. We used SEQRES data from the PDB to replace missing loops. Following that, to minimize steric conflicts, the Smart Minimizer Algorithm with the CHARMm force field was used to reduce the energy of all structures to an RMS gradient of 0.1 over 200 steps. We used STRIDE to estimate the secondary structures of ETEC's gyrA models [17]. The modeled structures were superimposed on the template crystal structure using the jCE method from the Combinatorial Extension technique. This was accomplished without changing the coordinate system of the atoms in the template [18].

Molecular docking

We selected amino acid alterations at positions 83 and 87 to form a sphere center in the ETEC receptor. Then, we selected amino acids that were within a radius of 10 Å from this sphere to identify the binding site and allow the ligand to freely rotate even in its fully extended shape. Utilizing the reduced receptor and ligand architectures, docking in LeadIt was accomplished with the aid of the FlexX incremental algorithm. This approach disassembles the ligand into its constituent pieces, uses a selection of those parts as anchors, and employs several placement strategies to do a comprehensive conformational study of the remaining ligand. In the present study, we performed a single interaction scan (SIS) using an entropy technique that depends on hydrophobic pockets with few contact sites. For protein-ligand collisions and intra-ligand conflicts, the default values of collision factor (0.6) and maximum permissible overlap volume (2.9 cubic Å) were applied. For each fragmentation and iteration, we received 200 distinct

alternatives. For every docking run, the top 10 ligand locations were identified, and conformations with the highest docking score (more negative) and the highest number of interactions were pursued further. The output score is calculated as follows using parameter-intensive Bohm's function: [19]

ΔG_{bind}= ΔG0 + ΔGhb$\sum h-bonds\ f\ (\Delta R, \Delta\alpha)$
+ΔGionic$\sum ionic\ interaction\ f\ (\Delta R, \Delta\alpha)$
+ ΔGlipo|Alipo| + ΔGrotNROT

On the right side of the equation, the values of ΔG are constants. Depending on the interaction geometry, ΔG0 represents the binding energy contribution that is unaffected by any particular interactions with the protein, hydrogen bonding, or ionic terms; deviations from the ideal distance R and ideal angle α result in penalties. The lipophilic term, |Alipo|, is proportional to the contact surface area between the non-polar atoms of the protein and the ligand, while the entropy term, which represents the expense associated with freezing the internal rotations of the ligand, is directly proportional to the number of rotatable bonds in the ligand (NROT).

MD Simulations

Molecular Dynamics in Amber 11.0 and Ambertools 1.5 were used to model the molecular system. The tLeap program within Ambertools was utilized to incorporate hydrogen atoms, and parameters were set in line with the AMBER FF99SB force field [20]. The TIP3P water model was used to solve the system in an octahedral box surrounded by a 15 A^ buffer [21]. Na^+ counterions were added to the systems to maintain neutrality. The energy of every molecular system in ETEC was minimized by three rounds of energy minimizations, each consisting of 1000 steps. The aforementioned systems comprised three different versions: 1) the original 1AB4 modeled complex; 2) the 1AB4 modeled complex featuring Ser to Leu at position 83; and 3) the 1AB4 modeled complex featuring Asp to Asn at position 87. The protein was subjected to energy reduction in two sets: 500 steps of steepest descent and 500 steps of conjugate gradient, with a time step of 2 fs, to eliminate close van der Waals connections. Locations were limited by 10 kcal-1é-2 and 2 kcal-1Å-2 during the first two minimization stages, respectively. On the other hand, no constraints were placed in place and the system was shrunk altogether in the third cycle. Following minimization, each system was heated gradually from 0 to 300 K after undergoing a continuous temperature equilibration at 300 K and 1 atm pressure for 100 ps. Following the stabilization of the thermodynamic properties, an isothermal isobaric ensemble (NPT, T = 300 K and P = 1 atm) was used for the 10-ns MD simulation, with an integration step of 2 fs and periodic boundary conditions for each system. The NPT conditions were maintained by using a Berendsen barostat) [22] and, a Langevin thermostat.[23] Using the SHAKE algorithm, [24] all covalent bonds containing hydrogen were limited.

Long-range electrostatic forces were addressed using the particle-mesh Ewald (PME) technique, and the charge grid interpolation on a cubic grid was carried out by setting the direct sum tolerance to 4.0 X 10^{-6} [25]. A charge grid spacing of about 1.0 A^ was used. Van der Waals interactions and short-range electrostatics were evaluated using a threshold based on 9.0 A^ atoms. Every two ps, we saved the trajectory coordinates for later examination. Following the execution of the MD simulations, the trajectories' root mean square fluctuations (RMSF) and root mean square deviations (RMSD) concerning every initial set of coordinates were analyzed. We were able to confirm the MD simulation process using the WT-gyrA model. The convergence of simulations was assessed for both ETEC molecular systems under investigation using tracking measures like energy components, root mean square deviation (RMSD) from the original modeled

structure, and root mean square fluctuation (RMSF) for WT-gyrA and all of the mutations.

MM-PBSA calculations

Using MM-PBSA and MM-GBSA, the usual methods, the free energies were calculated in AMBER 11. Free energies may be estimated in the final 5 ns of the MD simulation by analyzing 125 frames that were obtained for energetic analysis based on an average of the configurations obtained from 2500 frames at 20 ps.

The following equations were used to determine the binding free energy profiles for WT and each of the mutants:

$\Delta G_{bind} = G_{complex}\text{-}G_{receptor}\text{-}G_{ligand}$

$\Delta G_{bind} = E_{gas}+G_{sol}\text{-}T\Delta S$

$E_{gas} = E_{int}+E_{vdw}+E_{ele}$

$G_{sol} = G_{GB+}G_{SA}$

$G_{SA}+\Upsilon_{SASA}$

Where, S is the total solute entropy and T is the temperature. The Eint, Ele, and Evdw energies of a gas add up to its Egas value, which is the gas-phase energy of the gas. The parameters of the FF99SB force field terms are utilized to evaluate Egas. From the solvation-free energy (Gsol), polar and nonpolar solvation states can be further separated. Polarizable solvation contributions, GGB and GPB, are obtained by solving the Poisson Boltzmann (PB) and Generalised Born (GB) equations, respectively. The nonpolar solvation contribution (GSA) is estimated using a constant y value of 0.0072 kcal $mol^{-1}Å^{-2}$, and the solvent accessible surface area (SASA) is calculated using a water probe radius of 1.4 Å. The dielectric constant of the solvent was 80, whereas that of the solute was 1. The GB model, which is used in Amber11, was analyzed to find the interaction energy for every residue. This was done to determine the relative contribution of each amino acid to the overall binding free energy between the WT/MT of gyrA in ETEC and ciprofloxacin. We performed a decomposition analysis on the l25 frames that were recorded during the final 5 ns of the MD simulation. A "hotspot" amino acid was defined as an amino acid that contributed more than 0.5 kcal/mol in binding free energy. These hotspot amino acids have a major role in the complex's stability and its interaction with ciprofloxacin.

Residue Interaction Networks (RINs) analysis

The average structures derived from the most recent 5 ns trajectories of both ETEC were used to produce the RINs. The Reduce software adds hydrogen atoms to the input structure by the use of local geometry [26]. Small-probe contact dot surfaces are used by PROBE to assess the atomic packing of the amino acids and identify which ones interact with each other [27]. Several scoring functions are used by PROBE to quantify non-covalent interactions, including pi-pi interactions, hydrogen bonds, interatomic contact, and salt bridges. RINalyzer was used to view the RINs generated by the averaged MD structures [28]. We may identify network changes that correlate with physicochemical property changes in the structures by comparing many RINs.

Principal component analysis (PCA)

Essential dynamics (ED) calculations were performed using the principal component analysis (PCA) technique by minimizing the dimensionality of the MD simulations data to examine the direction and amplitude of the main movements of MD trajectories. Principal component analysis (PCA) may be used to identify an important subspace that is then used in normal modes analysis to examine the observable motions associated with the large-scale vibrational modes of atomic groups [29]. The configurational space is constructed via principal component analysis (PCA), which generates a covariance matrix (C) using a new set of coordinates and an orthogonal linear transformation. Principal components (PC) and related eigenvectors (Vi), or eigenvalues

(λi), are obtained by diagonalizing the covariance matrix. Vi, which also denotes the motion's direction, vectorically describes each component of the motion, and λi represents the amplitude of the eigenvectors along the multidimensional space.

Proj $[M, V_i] = M_\alpha.Vi$

Following the superimposition of M with the reference structure, each structure contains a Mα Cα atom. Projections are used to visualize the time-dependent motions of the components in a particular vibrational mode. Principal component analysis (PCA) was performed on two models using the PCAsuite software. ETEC included the mutants S83L/D87N, WT, and S83L.

RESULT AND DISCUSSION

Structural stability analysis

The homology modeling technique was utilized to determine the ETEC gyrA crystal structure because it was not available. A 91.2% identical template from *E. coli* gyrA was used to build the structure. To learn more about the atomic mechanism causing gyrA resistance to fluoroquinolones, we performed molecular dynamics simulations of WT and MT gyrA complexes from E. coli with ciprofloxacin. Computational simulations were conducted to support experimental results of higher MICs observed in clinical isolates carrying S83L and S83L/D87N mutations in WT and MT gyrA, which were docked against ciprofloxacin. We measured the time-dependent RMSDs of the backbone atoms concerning the appropriate energy-minimized structure to assess the conformational flexibility of the WT and MT structures. We validated the structure of the model with the lowest DOPE score based on its stereo-chemical properties using Verify3D and PROCHECK. 99.8% of residues are in the permitted zones, while 67.3% are in the most desirable places.

Composition of the secondary structure

As averaged by the ensemble, we provide in Figure 2 the secondary-structure populations of each amino acid residue. Although the conformations of WT and MT variants appear to be dominated by α-helices and turns, small quantities of regular secondary structures, such as β-sheet and helical structures, are seen. The pi-helix and parallel sheet populations are almost nonexistent for all systems that were evaluated. The helical content is significantly higher in all molecular systems than the β-sheet and turn contents [30]. None of the secondary structural richness differences between MT's ensemble averaged structures and WT could be seen. The WT and MT complexes' backbone conformations remain mostly unchanged due to the alterations. Y122 is located in the enzymatic region that controls gyrA's DNA-dependent ATPase activity. In quinolone resistance-associated gyrA mutants, we utilized VMD to investigate the enzymatic site and structural changes to the catalytic residue and surrounding active site residues (Figure 3).

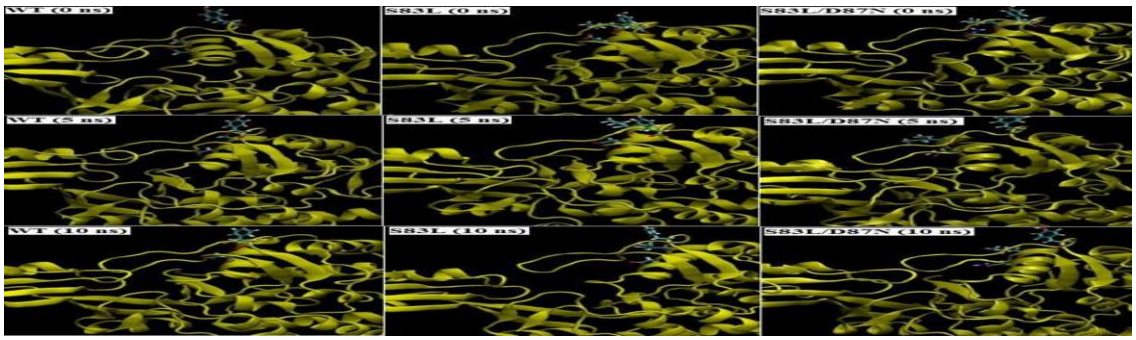

Fig. 2 Discovered conformational alterations in the catalytic residue Y122 and the mutated residues S83 and D87 at 0 ns (the beginning of the production phase), 5 ns, and 10 ns during the MD simulation in the WT (Column 1), S83L mutant (Column 2), and S83L/D87N mutant (Column 3).

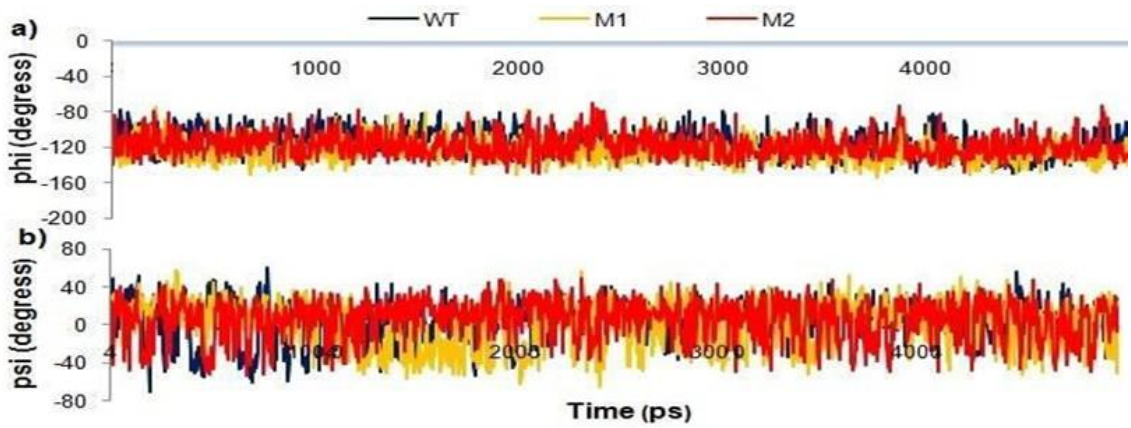

Fig. 3 Rotation of dihedral bond angles with time a) Dihedral angle phi b) Dihedral angle psi in the WT, S83L mutant, and S83L/D87N mutant during the MD simulation course. The dihedral angle of catalytic residue Y122 remains very steady during simulations, indicating that there hasn't been any significant conformational change.

MM-PB(GB)/SA binding independent energy simulations

Using MM-PB(GB)/SA methods, the free energy differences between WT and MT were evaluated. 125 frames from the most recent 5-ns simulation were analyzed to calculate the binding energy. The anticipated binding energies and the breakdown of the energy components for several simulated systems are shown in Table 1. In terms of total binding free energy, both methods often demonstrate a tendency toward lower binding affinities in MT as opposed to WT. When both methods were used, the binding energy (ΔGbinding) in the S83L/D87N double mutant dropped dramatically. GyrA has reduced binding affinities when mediated by mutations, which is when ciprofloxacin binds to it more efficiently. Ciprofloxacin resistance and MIC values are markedly increased by S83L and S83L/D87N, according to both experimental evidence and computational estimates of binding affinities. When comparing WT gyrA to both MT, it is evident that the electrostatic contribution (ΔEELE) and projected van der walls (ΔEVDW) are slightly higher. Table 1 indicates that the components ΔEVDW and ΔEELE are responsible for the majority of the positive contributions.

Table 1 Free binding energy profile of ciprofloxacin complexed with wild-type and S83L, S83L/D87N mutant forms of gyrA, based on MM-PB(GB)/SA

Contribution	WT	S83L	S83L/D87N
ΔE_{INT}	0	0	0
ΔE_{VDW}	-24.2421	-13.4977	-5.6295
ΔE_{ELE}	-110.813	-40.6163	-33.5151
ΔE_{GAS}/ ΔE_{MM}	-135.055	-54.114	-39.1446
ΔG_{SOL-NP}	-2.5072	-0.8743	0.1548
ΔG_{PB}	123.253	45.0921	34.9382
$\Delta G_{SOLV, PB}$	120.746	44.2177	35.0931
$\Delta G_{ELE, PB}$	12.44	4.4758	1.4231
$H_{TOT, PB}$	-14.3093	-9.8963	-4.0515
ΔG_{GB}	121.811	46.6201	36.6038
$\Delta G_{SOLV, GB}$	118.514	44.7953	35.8509
$\Delta G_{ELE\ GB}$	10.9982	6.0038	3.0887
$H_{TOT, GB}$	-16.5413	-9.3187	-3.2937

Binding energy reduction per residue

By analyzing the binding energy per residue, we can determine which residues in the wild-type and mutant variants of gyrA account for the majority of the binding. Figure 4 illustrates how each hot-spot residue contributes to the polar and non-polar interaction terms by comparing the protein-ligand interaction spectra from the WT and MT models. The energy breakdown research revealed that amino acids K42, H45, R91, L98, S172, G173, and I174 played important roles in the ciprofloxacin-bound WT complex. A change in the van der Waals contribution of hot-spot residues is primarily responsible for the drop in overall interaction energy in MT models. While the substitution of S83L for L at position 83 in the double mutant S83L/D87N improves binding at the mutation site (Total Score: -0.609 kcal/mol; van der Waals Score: -0.88 kcal/mol), it decreases overall binding energy (Table 1) because the substitution harms the binding affinity of nearby residues. This improvement is most likely due to stronger hydrophobic interactions with the L-side chain.

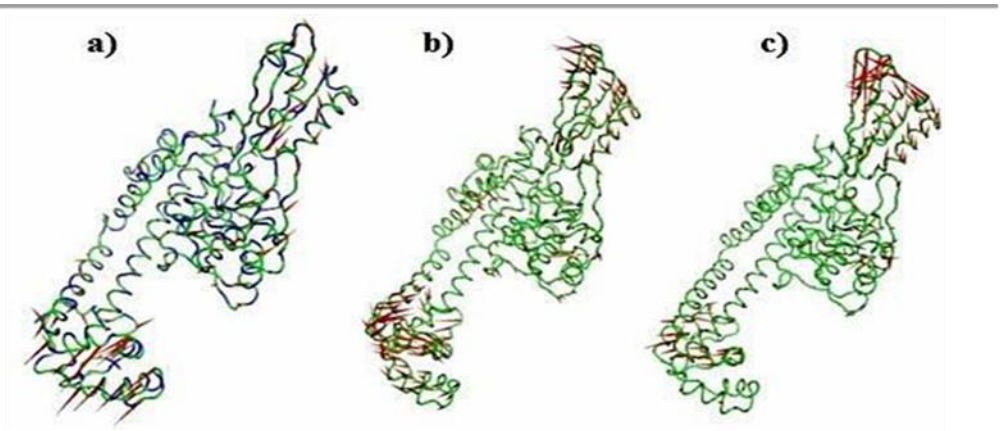

Fig. 4 Porcupine plot displays the first eigenvector for the following three mutants: a) S83L, b) WT, and c) S83L/D87N. It was obtained using principal component analysis (PCA) from the last five nanoseconds of the MD simulations.

PCA (Principal component analysis)

The final 5 ns trajectories of both the WT and MT complexes were submitted to principal component analysis (PCA) to determine the dominant movements. Figure 5 depicts a porcupine plot for the ciprofloxacin-bound WT and MT complexes in the direction of the first principal component, demonstrating the significant divergence in the overall pattern of global movements between the three systems. Typically, the three unique domains of N-terminal regions (NTD) demonstrated the most pronounced motions, as indicated by huge arrows. The HTH motif, located in the CAP domain, mediates contact with DNA targets [31]. The CAP domain in WT mostly moved upwards, however, in S83L there were no obvious motions, and in the twin mutant S83L/D87N there were random movements. It was discovered that the CAP domain in WT was considerably more flexible. The tower domain offers structural support and a DNA binding site, whereas the CAP domain functions as a support system. The tower domain in WT typically migrated upward, whereas in S83L and S83L/D87N it moved leftward, downward, and leftward. The ribbon indicates the protein backbone. Arrows indicate residue-dominant movements. Each arrow's size shows the magnitude of the relevant eigenvalue, and it also represents the direction of the eigenvector. According to reference, [32] the bending of two α-helices that link the dimerization domain to the CTD and

the tower domain leads gyrA to alternate between open and closed positions. We observed that the direction and amplitude of major movements in all three domains were significantly altered in MT variants compared to WT structures. Trajectories' overall conformations from the most recent 5 ns of simulation differed between structures.

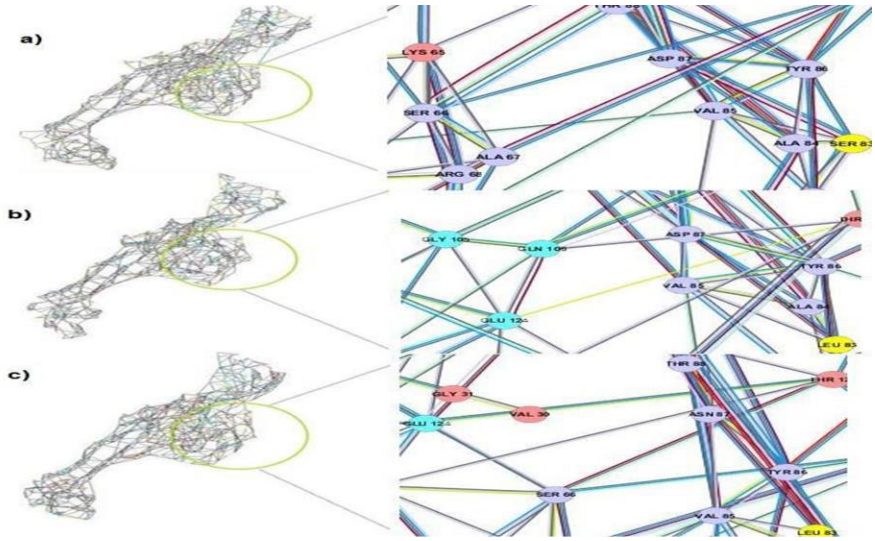

Fig. 5 Residue interaction networks (RINs) in three distinct mutant forms—wild-type (WT), S83L, and S83L/D87N— compared with ciprofloxacin. Network changes are visible at the catalytic residue Y122 and the mutant QRDR residues S83 and D87 in a magnified picture.

RIN analysis

A RIN was created using the representative structures of each chemical system's final 5 ns trajectories to identify critical residue interactions and compare the differences between distinct WT and MT models. The S83L/D87N mutant has no connections in the Q106, T123, or E124 interaction networks, but the interaction sub-network containing residues 30-34 collapses. Mutations S83L and D87N appear to have influenced the drug-binding landscape by disrupting the RIN of WT gyrA.

CONCLUSION

The continuously growing number of computer platforms examining the structural implications of the mutations has become easier. Using explicit-water MD simulations, we conducted a comprehensive study to explore the molecular basis of gyrA mutations associated with quinolone resistance. The MT and WT routes examined the identical conformational space, and RMS fluctuation, secondary structure conservation, and RMS deviation all showed no discernible variations. In any case, complicated mutations show up as altered dominant motions and significant disruptions to the residue interaction network, which have the potential to destabilize the active-site conformation and lessen ligand binding efficiency. The genotype-phenotype association of gyrA SNPs associated with quinolone resistance is adequately demonstrated in this study. The results of this study provide information on the role of gyrA mutations in the fight against ETEC-resistant bacteria, which may impact the creation of novel treatment strategies based on these mutations.

Declaration by Authors

Acknowledgement: None
Source of Funding: None
Conflict of Interest: The authors declare no conflict of interest.

REFERENCES

1. Mun Huang W. Bacterial diversity based on type II DNA topoisomerase genes. *Annu. Rev. Genet*. 1996 Dec;30(1):79-107.
2. Khan T, Sankhe K, Suvarna V, Sherje A, Patel K, Dravyakar B. DNA gyrase inhibitors: Progress and synthesis of potent compounds as antibacterial agents. *Biomed. Pharmacother*. 2018 Jul 1;103: 923-938.
3. Reece RJ, Maxwell A. DNA gyrase: structure and function. *Crit. Rev. Biochem. Mol. Biol*. 1991 Jan 1;26(3-4):335-375.
4. Cabral JH, Jackson AP, Smith CV, Shikotra N, Maxwell A, Liddington RC. Crystal structure of the breakage–reunion domain of DNA gyrase. *Nature*. 1997 Aug 28;388(6645):903-6.
5. Fàbrega A, Madurga S, Giralt E, Vila J. Mechanism of action of and resistance to quinolones. *Microb. Biotechnol*. 2009 Jan;2(1):40-61.
6. Millanao AR, Mora AY, Villagra NA, Bucarey SA, Hidalgo AA. Biological effects of quinolones: a family of broad-spectrum antimicrobial agents. *Molecules*. 2021 Nov 25;26(23):7153.
7. Spencer AC, Panda SS. DNA Gyrase as a Target for Quinolones. *Biomedicines*. 2023 Jan 27;11(2):371.
8. Juma BW. Molecular Epidemiology of enterotoxigenic *Escherichia coli* and other enteric pathogenic bacteria isolated in Machakos District Hospital Machakos County. 2013.
9. Ena J, del Mar Lopez-Perezagua M, Martınez-Peinado C, de los Angeles Cia-Barrio M, Ruız-Lopez I. Emergence of ciprofloxacin resistance in Escherichia coli isolates after widespread use of fluoroquinolones. *Diagn. Microbiol. Infect. Dis*. 1998 Feb 1;30(2):103-107.
10. Yoshida H, Bogaki MA, Nakamura MI, Yamanaka LM, Nakamura SH. Quinolone resistance-determining region in the DNA gyrase gyrB gene of *Escherichia coli*. *Antimicrob. Agents Chemother*. 1991 Aug;35(8):1647-1650.
11. Jacoby GA. Mechanisms of resistance to quinolones. *Clin. Infect. Dis*. 2005 Jul 15;41(Supplement_2): S120-S126.
12. Isenbarger DW, Hoge CW, Srijan A, Pitarangsi C, Vithayasai N, Bodhidatta L, Hickey KW, Cam PD. Comparative antibiotic resistance of diarrheal pathogens from Vietnam and Thailand, 1996-1999. *Emerg. Infect. Dis*. 2002 Feb;8(2):175.
13. Mendez Arancibia E, Pitart C, Ruiz J, Marco F, Gascon J, Vila J. Evolution of antimicrobial resistance in enteroaggregative *Escherichia coli* and enterotoxigenic *Escherichia coli* causing traveller's diarrhoea. *J. Antimicrob. Chemother*. 2009 Aug 1;64(2):343-347.
14. Bolton EE, Wang Y, Thiessen PA, Bryant SH. PubChem: integrated platform of small molecules and biological activities. InAnnual reports in computational chemistry 2008 Jan 1 (Vol. 4, pp. 217-241). Elsevier.
15. Eisenberg D, Lüthy R, Bowie JU. [20] VERIFY3D: assessment of protein models with three-dimensional profiles. InMethods in enzymology 1997 Jan 1 (Vol. 277, pp. 396-404). Academic Press.
16. Laskowski RA, MacArthur MW, Moss DS, Thornton JM. PROCHECK: a program to check the stereochemical quality of protein structures. *J. Appl. Crystallogr*. 1993 Apr 1;26(2):283-291.
17. Frishman D, Argos P. Knowledge-based protein secondary structure assignment. *Proteins: Struct., Funct., Bioinf*. 1995 Dec;23(4):566-579.
18. Shindyalov IN, Bourne PE. Protein structure alignment by incremental combinatorial extension (CE) of the optimal path. *Protein Eng*. 1998 Sep 1;11(9):739-747.
19. Böhm HJ. The development of a simple empirical scoring function to estimate the binding constant for a protein-ligand complex of known three-dimensional structure. *J. Comput. Aided Mol. Des*. 1994 Jun;8:243-256.
20. Hornak V, Abel R, Okur A, Strockbine B, Roitberg A, Simmerling C. Comparison of multiple Amber force fields and development of improved protein backbone parameters. *Proteins: Struct., Funct., Bioinf*. 2006 Nov 15;65(3):712-725.
21. Jorgensen WL, Chandrasekhar J, Madura JD, Impey RW, Klein ML. Comparison of simple potential functions for simulating liquid water. *J. Chem. Phys*. 1983 Jul 15;79(2):926-935.
22. Berendsen HJ, Postma JV, Van Gunsteren WF, DiNola AR, Haak JR. Molecular dynamics

with coupling to an external bath. *J. Chem. Phys*. 1984 Oct 15;81(8):3684-3690.
23. Davidchack RL, Handel R, Tretyakov MV. Langevin thermostat for rigid body dynamics. *J. Chem. Phys*. 2009 Jun 21;130(23).
24. Ryckaert JP, Ciccotti G, Berendsen HJ. Numerical integration of the cartesian equations of motion of a system with constraints: molecular dynamics of n-alkanes. *J. Comput. Phys*. 1977 Mar 1;23(3):327-341.
25. Darden T, York D, Pedersen L. Particle mesh Ewald: An N· log (N) method for Ewald sums in large systems. *J. Chem. Phys*. 1993 Jun 15;98(12):10089-10092.
26. Word JM, Lovell SC, LaBean TH, Taylor HC, Zalis ME, Presley BK, Richardson JS, Richardson DC. Visualizing and quantifying molecular goodness-of-fit: small-probe contact dots with explicit hydrogen atoms. *J. Mol. Biol*. 1999 Jan 29;285(4):1711-1733.
27. Word JM, Lovell SC, Richardson JS, Richardson DC. Asparagine and glutamine: using hydrogen atom contacts in the choice of side-chain amide orientation. *J. Mol. Biol*. 1999 Jan 29;285(4):1735-1747.
28. Doncheva NT, Klein K, Domingues FS, Albrecht M. Analyzing and visualizing residue networks of protein structures. *Trends Biochem Sci*. 2011 Apr 1;36(4):179-182.
29. Amadei A, Linssen AB, Berendsen HJ. Essential dynamics of proteins. *Proteins: Struct., Funct., Bioinf*. 1993 Dec;17(4):412-425.
30. William H. VMD-visual molecular dynamics. *J. Mol. Graph*. 1996; 14:33-38.
31. Berger JM, Fass D, Wang JC, Harrison SC. Structural similarities between topoisomerases that cleave one or both DNA strands. *Proc Natl Acad Sci*. 1998 Jul 7;95(14):7876-7881.
32. Corbett KD, Schoeffler AJ, Thomsen ND, Berger JM. The structural basis for substrate specificity in DNA topoisomerase IV. *J. Mol. Biol*. 2005 Aug 19;351(3):545-561.

How to cite this article: Nitin Jumnani. Repercussions on quinolone resemblance in enterotoxigenic *E. coli* gyrA mutants: molecular dynamics simulations and residue interaction network analysis. *Int J Health Sci Res.* 2024; 14(7):100-110. DOI: *10.52403/ijhsr.20240714*

******